Journal of
Mechanics of
Materials and Structures

DYNAMICS AND STABILITY ANALYSIS OF AN AXIALLY MOVING BEAM IN AXIAL FLOW

Yan Hao, Huliang Dai, Ni Qiao, Kun Zhou and Lin Wang

Volume 15, No. 1 January 2020

msp

JOURNAL OF MECHANICS OF MATERIALS AND STRUCTURES
Vol. 15, No. 1, 2020
dx.doi.org/10.2140/jomms.2020.15.37

DYNAMICS AND STABILITY ANALYSIS OF AN AXIALLY MOVING BEAM IN AXIAL FLOW

YAN HAO, HULIANG DAI, NI QIAO, KUN ZHOU AND LIN WANG

The present study focuses on investigating dynamics and stability of an axially moving beam subjected to axial flows. The axially moving beam is simply-supported at both ends. The added mass of fluid attached to the beam and the nonlinear additional deflection-dependent axial force are considered in deriving the governing equation of motion. Firstly, the stability analysis is performed with consideration of the effects of parameters such as axial flow velocity, the speed of axially moving beam and slenderness ratio of the beam. It is indicated that the beam loses stability via buckling or flutter at a critical speed of moving beam which is associated with variations of system parameters. Subsequently, the nonlinear dynamic responses of the beam for increasing moving speed under different axial flow velocities are investigated in detail. Results show that the beam can successively experience buckling and flutter behaviors. In addition, effects of system parameters like mass ratio, slenderness ratio, and pretension on instability mode, buckling displacement and flutter amplitude of the beam are explored to obtain their sensitivity to dynamics of the moving beam. These findings provide an important guidance for designing axially moving structures in engineering applications.

1. Introduction

Axially moving structures (e.g., axially moving beams [Ghayesh et al. 2013a], belts [Hedrih 2007], strings [Chen et al. 2009], plates [Ghayesh et al. 2013b] can be applied in many engineering devices, such as magnetic tapes, aerial cables, power transmission belts and band saw blades. Owing to the widespread applications, the dynamics of elastic or viscoelastic beams axially moving at a certain speed have attracted increasing attention in the past decades from both academic and engineering realms. Hitherto, a great deal of research works on the dynamical behavior of axially moving material has been reported. One can get a general understanding of this field in [Mote Jr. 1968; Wickert and Mote 1988; Chen 2005; Marynowski and Kapitaniak 2014; Païdoussis and Li 1993].

Problems of interaction between axially moving structures and fluid have significant applications in shipping and ocean engineering, underwater equipment and aeronautical industries. Acoustic streamers used in ocean exploration [Telford et al. 1976], steel strip in continuous hot-dip galvanizing process [Li et al. 2013; Wang et al. 2016] and the underwater towed slender structures [Brown 2006; Kyriakides and Corona 2007] are typical examples. There are many fluid forces applied on structures and they have a great effect on the dynamics and stability of the axially moving structure system. In recent decades, many researches about axially moving structures like plates or beams under flow conditions have been conducted. Frondelius et al. [2006] investigated the interaction of an axially moving band and

Ni Qiao is the corresponding author.
Keywords: axially moving beam, axial flow, stability analysis, buckling, flutter.

surrounding fluid through boundary layer theory. Their results are significantly different from the earlier work. The dynamic behavior of axially moving plates and membranes immersed in axially flowing ideal fluid was investigated in [Banichuk et al. 2010; 2011]. Taleb and Misra [1981] investigated the dynamics of an axially deploying beam submerged in dense fluid, and Gosselin et al. [2007] improved Taleb's work by taking the axial added mass coefficient into account. Inspired by their works, Yan et al. [2016] investigated the dynamics of an extending beam attached to an axially moving base immersed in dense fluid. They found that the increase of velocity of the moving base can stabilize the system. Huo and Wang [2016] developed a theoretical model for an axially deploying/retracting cantilevered pipe conveying fluid and carried out a linear analysis. Then, Yan et al. [2018] tackled the same problem as Huo and Wang [2016]. They investigated the nonlinear dynamics of a sliding pipe conveying fluid. Wang and Ni [2008] conducted a linear study on the vibration and stability of an axially moving beam immersed in fluid using the differential quadrature method (DQM). The natural frequencies of the system were obtained for three different boundary conditions, i.e., hinged-hinged, fixed-fixed and hybrid supports with torsion spring. Afterwards, Ni et al. [2014] investigated the linear vibration and stability of a cantilevered beam attached to an axially moving base which was immersed in fluid. In this work, a transformation between absolute and moving coordinates was introduced to construct the theoretical model. In addition, a study on an underwater slender beam with two axially moving supports has been done in [Li et al. 2015b]. By utilizing the same modeling method as in their previous work, nonlinear governing equations are obtained and rich dynamic behaviors are detected. Païdoussis [1968; 1970] conducted some experiments and constructed linear theoretical model to study the dynamics and stability of towed cylinders. Qualitative agreement between experiment and theory was reached. Moreover, Païdoussis et al. [2002], Lopes et al. [2002] and Semler et al. [2002] conducted a fully nonlinear analytical investigation on the dynamics of a beam in axial flow. De Langre et al. [2007] proposed a simple model for the dynamical behaviour of long flexible cylinders in axial flow. Numerical results and experimental data show that flutter may exist for very long cylinders. Kheiri et al. [2013a; 2013b] derived three-dimensional linear equations of motion with consideration of cross-current effect to investigate the dynamics of long pipes towed underwater. Results show that the pipe may lose stability by divergence and at higher flow velocities by flutter. It should be noted that Kheiri et al. [2013c; 2015] developed a nonlinear model for a towed flexible slender cylinder via Hamilton's principle and conducted an experiment. The numerical results agree well with experimental observations, which show that a sufficiently blunt tail end-piece has a significant stabilizing effect.

In addition, Wang and Zu [2017a] investigated the instability of a viscoelastic plate, which moves longitudinally at variable velocity and is in contact with ideal liquid, by using multiple-scale method. Considering a plate made of functionally graded materials, Wang and Zu [2017b] and Wang [2018] investigated the multifield coupled dynamics of an axially moving system. Li et al. [2015a] studied the internal resonance of an axially moving unidirectional plate which is partially immersed in fluid and under foundation displacement excitation. More recently, Li et al. [2018] tackled a similar problem as that in their previous work [Li et al. 2015a], while this latest work was mainly concerned with the characteristics of combination resonances and its stability of this fluid-structure coupling system under two frequency excitations.

However, the previous studies on axially moving structures in fluid did not consider the flow velocity in the axial direction (i.e., the axial flow velocity equals to zero). Although some researches [Dowling 1988; Kim and Perkins 2002] mentioned the axial flow, the axial flow effect in their researches is actually

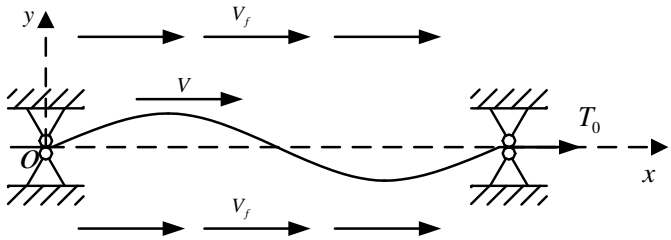

Figure 1. Schematic of an axially moving beam in axial flow.

due to the underwater structures being towed or axially moving themselves. That's to say, the external axial flow velocity is indeed zero. And it is noted that an axially moving beam in external axial flow with nonzero velocity is a common problem in ocean engineering and other applications. Hence, it is significant to take the axial flow into account when investigating the dynamic behaviors of axially moving structures. Motivated by this, the present study focuses on investigating the dynamics of axially moving beams in axial flow with nonzero velocity.

In this paper, we consider an axially flexible beam moving at the speed of V with both ends supported. The axially moving beam is simultaneously subjected to axial flow with velocity V_f, as shown in Figure 1. A nonlinear governing equation of motion will be derived by using Newtonian method and discretized via Galerkin's technique. Based on Runge–Kutta numerical method, the dynamical behavior and vibration responses of the beam are obtained.

2. Theoretical modeling

2.1. ***Assumptions and kinetic description.*** The axially moving beam indicated in Figure 1 has length l, diameter D, area moment of inertia I, and mass per unit length m. A complex elasticity modulus of material is utilized, $E_0 I(1 + \gamma\partial/\partial t)$, where γ is a coefficient of internal dissipation assumed to be viscoelastic and of the Kelvin–Voigt type. The simply-supported beam is travelling at a speed of V. It is subjected to a pretension T_0 and an axial flow velocity V_f. The density of the fluid is ρ. In the present study, we assume the fluid is incompressible and the mean flow velocity is constant. Although the deflections of the beam may be large, the strains are small. Furthermore, the influences of pressure drop, gravity, shear deformation and rotary inertia of the beam are ignored for a simplified analysis.

In this work, the longitudinal and transverse displacements of the beam element are denoted by $u(x, t)$ and $w(x, t)$, respectively. Moreover, it should be noted that longitudinal displacements are one order of magnitude smaller than the lateral ones, hence $u(x, t)$ can be ignored in the Newtonian approach. Then, the velocity and acceleration of the same element can be easily obtained [Ghayesh 2012; Yan et al. 2016]:

$$V_{bx} \approx V, \quad a_{bx} \approx \dot{V}, \quad B_{by} = \frac{\partial w}{\partial t} + V\frac{\partial w}{\partial x}, \quad a_{by} \approx \left(\frac{\partial}{\partial t} + V\frac{\partial}{\partial x}\right)^2 w, \tag{1}$$

where the subscripts bx and by stand for components of the velocity or acceleration of the beam element along the x- and y-direction, respectively. The over-dot denotes the derivative with respect to time.

2.2. ***Added mass and inviscid hydrodynamic forces.*** For this system, the lateral virtual mass per unit length is considered and defined as $m_v = \rho(\frac{1}{4}\pi D^2)$. However, in the axial direction of the beam, according to Païdoussis [2016] and Gosselin et al. [2007], the mass of the fluid attached to the beam is smaller than that of the lateral-direction virtual mass. Therefore, an "axial added mass coefficient" β is introduced to modify axial virtual mass as βm_v, where β varies between 0 and 1.

In the lateral direction, the resultant relative velocity between beam and fluid flowing past it can be expressed as [Lighthill 1960]

$$V_r = \frac{\partial w}{\partial t} + (V + V_f)\frac{\partial w}{\partial x}. \tag{2}$$

We suppose that this flow has momentum $m_v V_r$ per unit length of beam [Païdoussis 1998], the rate of change of this momentum per unit length is $[\partial/\partial t + (V + V_f)\cdot\partial/\partial x]\, m_v V_r$ and brings about an equal and opposite lateral force on the beam [Lighthill 1960]. According to Gosselin et al. [2007], this lateral inviscid hydrodynamic force can be rewritten as

$$F_{AL} = m_v\left(\frac{\partial}{\partial t} + \beta(V_f + V)\frac{\partial}{\partial x}\right)^2 w. \tag{3}$$

According to Païdoussis [2016], the dynamics of cylinder in axial flow is principally controlled by the inviscid force, which can be expressed as $m_v(\partial/\partial t + \beta V_f \cdot \partial/\partial x)^2 w$. Thus, it is supposed that the effect of V is simply to change V_f to $V_f + V$, and its effect on the dynamics of axially moving beam in axial flow can be expected to be quantitative rather than qualitative, as compared to a stationary cylinder in axial flow.

Owing to the fact that the beam is axially moving with speed V and immersed in fluid, the momentum per unit length of the fluid attached on the beam in the axial direction is $\beta m_v V$. Hence the axial inviscid hydrodynamic force F_{AD} can be obtained as

$$F_{AD} = \beta m_v \dot{V}. \tag{4}$$

2.3. ***Viscous forces.*** According to Taylor's work [Taylor 1952], the viscous forces per unit length of the beam along normal and longitudinal directions are

$$F_N = \frac{1}{2}\rho D U^2\big(C_{D_p}\sin^2 i + C_f \sin i\big), \tag{5}$$

$$F_L = \frac{1}{2}\rho D U^2 C_f \cos i, \tag{6}$$

where C_f and C_{D_p} are frictional and form drag coefficients, and i is the angle of incidence of the beam.

After straightforward but tedious manipulations and a linearization procedure, one can get the viscous forces in their simplest form as

$$F_L = \frac{1}{2}\frac{m_v}{D}(V_f - V)^2 c_f \operatorname{sgn}(V_f - V), \tag{7}$$

$$F_{Ny} = \frac{1}{2}\frac{m_v}{D}\left[c_f |V_f - V|\left(\frac{\partial w}{\partial t} + V_f\frac{\partial w}{\partial x}\right) + c_d\left(\frac{\partial w}{\partial t} + V\frac{\partial w}{\partial x}\right)\right], \tag{8}$$

where F_{Nx} can be neglected for its high order, and $\mathrm{sgn}(V_f - V)$ is a sign function, i.e., $\mathrm{sgn}(V_f - V) = 1$ if $V_f > V$; $\mathrm{sgn}(V_f - V) = -1$ if $V_f < V$; $\mathrm{sgn}(V_f - V) = 0$ if $V_f = V$. Details for derivation of the above expressions of (7) and (8) are given in Appendix A.

It is obvious that the dynamics of structures in axial flow also depends on the viscous forces. However, viscous forces do not control the stability behaviour and just modify it [Païdoussis 2016]. One can find that the expressions of viscous force shown above contain terms with $V_f - V$, which just shows that the model of an axially moving beam in axial flow is quite different from that of a stationary cylinder in axial flow, i.e., the case of $V = 0$.

2.4. ***Newtonian approach.*** An element δx of beam is chosen for modeling the dynamic equations, as shown in Figure 2. Let the shear force, axial tension and bending moment be denoted as Q, T and M, respectively. The inertia forces along the x- and y-directions are denoted as F_{Ix} and F_{Iy}. Summing forces in the x- and y-directions and the moment in the out-plane direction, yielding

$$F_{Ix} - \frac{\partial T}{\partial x} - F_L - F_{Nx} + F_{AD} = 0, \tag{9}$$

$$F_{Iy} + F_{Ny} + F_{AL} - F_L \frac{\partial w}{\partial x} - \frac{\partial}{\partial x}\left(Q + T\frac{\partial w}{\partial x}\right) = 0, \tag{10}$$

$$Q = -E_0 I\left(1 + \gamma\frac{\partial}{\partial t}\right)\frac{\partial^3 w}{\partial x^3}, \tag{11}$$

where F_{Nx} and F_{Ny} denote projections of normal viscous force on x- and y-directions, respectively.

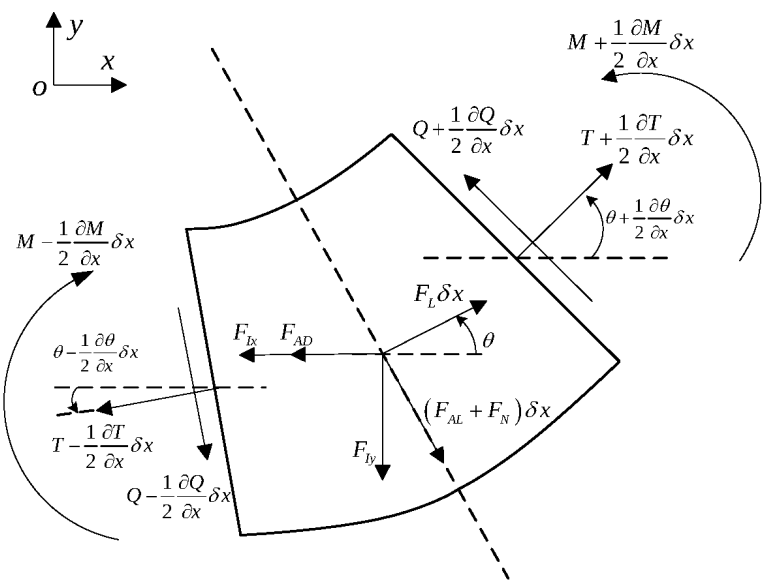

Figure 2. An element δx of the beam with forces and moments acting on it.

By substituting (3), (4), (7) and (8) into (9) to (11), and using the relationships $F_{Ix} = ma_{bx}$ and $F_{Iy} = ma_{by}$, the following equations can be obtained:

$$m\dot{V} + \beta m_v \dot{V} - \frac{1}{2} c_f \frac{m_v}{D} (V_f - V)^2 \operatorname{sgn}(V_f - V) - \frac{\partial T}{\partial x} = 0, \tag{12}$$

$$\begin{aligned} E_0 I \left(1 + \gamma \frac{\partial}{\partial t}\right) \frac{\partial^4 w}{\partial x^4} + m \left(\frac{\partial}{\partial t} + V \frac{\partial}{\partial x}\right)^2 w + m_v \left(\frac{\partial}{\partial t} + \beta (V_f + V) \frac{\partial}{\partial x}\right)^2 w \\ + \frac{1}{2} \frac{m_v}{D} \left[c_f |V_f - V| \left(V_f \frac{\partial w}{\partial x} + \frac{\partial w}{\partial t} \right) + c_d \left(\frac{\partial w}{\partial t} + V \frac{\partial w}{\partial x} \right) \right] \\ - \frac{1}{2} c_f \frac{m_v}{D} (V_f - V)^2 \frac{\partial w}{\partial x} \operatorname{sgn}(V_f - V) - \frac{\partial}{\partial x} \left(T \frac{\partial w}{\partial x} \right) = 0. \end{aligned} \tag{13}$$

By integrating (12) from x to l, and replacing the integration constant by the value of pretension T_0 at the end of the beam [Wang and Ni 2008], the axial tension can be obtained as

$$T(x) = -\left[(m + \beta m_v) \dot{V} - \frac{1}{2} c_f \frac{m_v}{D} (V_f - V)^2 \operatorname{sgn}(V_f - V) \right] (l - x) + T_0. \tag{14}$$

Substituting (12) and (14) into (13), the linear equation of motion can be obtained as

$$\begin{aligned} & E_0 I \left(1 + \gamma \frac{\partial}{\partial t}\right) \frac{\partial^4 w}{\partial x^4} \\ & + \left(m_v \beta^2 (V_f + V)^2 + m V^2 + \left[(m + \beta m_v) \dot{V} - \frac{1}{2} c_f \frac{m_v}{D} (V_f - V)^2 \operatorname{sgn}(V_f - V) \right] (l - x) - T_0 \right) \frac{\partial^2 w}{\partial x^2} \\ & + 2 \left(m_v \beta V_f + (m + \beta m_v) V \right) \frac{\partial^2 w}{\partial t \, \partial x} + \frac{1}{2} \frac{m_v}{D} (c_f |V_f - V| V_f + c_d V) \frac{\partial w}{\partial x} \\ & + \beta m_v \dot{V}_f \frac{\partial w}{\partial x} + \frac{1}{2} \frac{m_v}{D} (c_f |V_f - V| + c_d) \frac{\partial w}{\partial t} + (m + m_v) \frac{\partial^2 w}{\partial t^2} = 0. \end{aligned} \tag{15}$$

It is noted that this equation of motion can simplify into the governing equation for a cylindrical structure in axial fluid derived by Païdoussis [1998] when $V = 0$; also, it becomes the equation of motion for an axially moving beam if one removes the terms related to the fluid.

Moreover, the axial tension caused by the bending deflection should be taken into account if the order of amplitude of the transverse displacement is close to the order of the diameter of the beam [Li et al. 2015b]. Thus the additional nonlinear deflection-dependent axial force can be represented as

$$E_0 \left(1 + \gamma \frac{\partial}{\partial t}\right) \frac{A}{2l} \left(\frac{\partial w}{\partial x} \right)^2.$$

Then, an integral term

$$E_0 \left(1 + \gamma \frac{\partial}{\partial t}\right) \frac{A}{2l} \frac{\partial^2 w}{\partial x^2} \int_0^l \left(\frac{\partial w}{\partial x} \right)^2 dx,$$

should be added into (15) and the nonlinear governing equation for the beam system can be obtained as

$$\begin{aligned} &E_0 I\left(1+\gamma\frac{\partial}{\partial t}\right)\frac{\partial^4 w}{\partial x^4} \\ &\quad+\left(m_v\beta^2(V_f+V)^2+mV^2+\left[(m+\beta m_v)\dot{V}-\frac{1}{2}c_f\frac{m_v}{D}(V_f-V)^2\,\mathrm{sgn}(V_f-V)\right](l-x)\right. \\ &\qquad\left.-T_0-E_0\left(1+\gamma\frac{\partial}{\partial t}\right)\frac{A}{2l}\int_0^l\left(\frac{\partial w}{\partial x}\right)^2 dx\right)\frac{\partial^2 w}{\partial x^2} \\ &\qquad+2\big(m_v\beta V_f+(m+\beta m_v)V\big)\frac{\partial^2 w}{\partial t\,\partial x}+\frac{1}{2}\frac{m_v}{D}(c_f|V_f-V|V_f+c_d V)\frac{\partial w}{\partial x} \\ &\qquad+\beta m_v\dot{V}_f\frac{\partial w}{\partial x}+\frac{1}{2}\frac{m_v}{D}(c_f|V_f-V|+c_d)\frac{\partial w}{\partial t}+(m+m_v)\frac{\partial^2 w}{\partial t^2}=0. \end{aligned} \tag{16}$$

2.5. ***Nondimensionalization.*** After the following dimensionless variables and parameters:

$$\begin{gathered} \eta=\frac{w}{l},\quad \xi=\frac{x}{l},\quad \tau=\left(\frac{E_0 I}{m+m_v}\right)^{1/2}\frac{t}{l^2}=\alpha t,\quad v_f=\left(\frac{m_v}{E_0 I}\right)^{1/2}V_f l,\quad v=\left(\frac{m_v}{E_0 I}\right)^{1/2}Vl, \\ \varphi=\frac{m_v}{m+m_v},\quad \phi=\frac{m}{m_v},\quad \varepsilon=\frac{l}{D},\quad \bar{c}_d=\frac{c_d}{\alpha l},\quad \Gamma=\frac{T_0 l^2}{E_0 I},\quad \bar{\gamma}=\alpha\gamma, \\ \mu=\frac{Al^2}{I}=16\left(\frac{l}{D}\right)^2=16\varepsilon^2, \end{gathered} \tag{17}$$

are introduced in (16), the nonlinear equation of motion is obtained as

$$\begin{aligned} &\eta''''+\bar{\gamma}\dot{\eta}''''+\left(\phi v^2+\beta^2(v_f+v)^2+\left[(\phi+\beta)\varphi^{1/2}\dot{v}-\frac{1}{2}c_f\varepsilon(v_f-v)^2\,\mathrm{sgn}(v_f-v)\right](1-\xi)\right. \\ &\qquad\left.-\Gamma-\frac{\mu}{2}\int_0^1\eta'^2\,d\xi-\bar{\gamma}\mu\int_0^1\eta'\dot{\eta}'\,d\xi\right) \\ &\qquad+2\big((\phi+\beta)v+\beta v_f\big)\varphi^{1/2}\dot{\eta}'+\left[\frac{1}{2}\varepsilon(c_f|v_f-v|v_f+\bar{c}_d\varphi^{1/2}v)+\beta\varphi^{1/2}\dot{v}_f\right]\eta' \\ &\qquad+\frac{1}{2}\varepsilon(\varphi^{1/2}c_f|v_f-v|+\bar{c}_d\varphi)\dot{\eta}+\ddot{\eta}=0, \end{aligned} \tag{18}$$

where the over-dot and the prime denote the derivative with respect to τ and ξ, respectively.

3. Solutions via Galerkin's technique

The governing equation can be transformed into a set of ordinary equations (ODEs) via applying the Galerkin procedure, such that

$$\eta(\xi,\tau)=\sum_{j=1}^{N}\phi_j(\xi)\,q_j(\tau), \tag{19}$$

where N is the number of terms for Galerkin truncation. In this study, the eigenfunctions of a pinned-pinned beam are elected to be the admissible functions, i.e., $\phi_j(\xi)=\sqrt{2}\sin j\pi\xi$.

Substituting the above expression into (18), multiplying by $\phi_i(\xi)$ and integrating from 0 to 1 leads to

$$\boldsymbol{M}\ddot{\boldsymbol{q}} + \boldsymbol{C}\dot{\boldsymbol{q}} + \boldsymbol{K}\boldsymbol{q} + \boldsymbol{N}(\boldsymbol{q}) = 0, \tag{20}$$

where $\boldsymbol{M}$, $\boldsymbol{C}$, $\boldsymbol{K}$, $\boldsymbol{N}$ represent the structural mass matrix, damping matrix, stiffness matrix and nonlinear vector, respectively. The elements of these matrices are

$$\begin{aligned}
M_{ij} &= e_{ij} = \int_0^1 \phi_i\,\phi_j\,d\xi = \delta_{ij},\\
C_{ij} &= \frac{1}{2}\varepsilon(\varphi^{1/2}c_f|v_f - v| + \bar{c}_d\varphi)\,e_{ij} + \overline{\gamma}a_{ij} + 2\big((\phi+\beta)v + \beta v_f\big)\,\varphi^{1/2}d_{ij},\\
K_{ij} &= a_{ij} + \big(\phi v^2 + \beta^2(v_f+v)^2 + \Theta - \Gamma\big)b_{ij} - \Theta c_{ij} + \left[\frac{1}{2}\varepsilon(c_f|v_f - v|v_f + \bar{c}_d\,\varphi^{1/2}v) + \beta\varphi^{1/2}\dot{v}_f\right]d_{ij},\\
N(\boldsymbol{q}) &= -\frac{\mu}{2}\alpha_{ijkl}\,q_j\,q_k\,q_l - \overline{\gamma}\mu\,\alpha_{ijkl}\,q_j\,q_k\,\dot{q}_l,
\end{aligned} \tag{21}$$

where δ_{ij} is Kronecker delta and $\Theta = (\phi+\beta)\varphi^{1/2}\dot{v} - \frac{1}{2}c_f\varepsilon(v_f - v)^2\,\mathrm{sgn}(v_f - v)$.

Other coefficients in (21) are obtained as follows [Païdoussis 1998]:

$$\begin{aligned}
a_{ij} &= \int_0^1 \phi_1\,\phi_j''''\,d\xi = (j\pi)^4\delta_{ij}, \quad b_{ij} = \int_0^1 \phi_i\,\phi_j''\,d\xi = -(j\pi)^2\delta_{ij},\\
c_{ij} &= \int_0^1 \xi\phi_i\,\phi_j''\,d\xi = \begin{cases} \frac{4ij^3}{(j^2-i^2)^2}[1-(-1)^{j+1}] & i \neq j,\\ -\frac{1}{2}(j\pi)^2 & i = j,\end{cases}\\
d_{ij} &= \int_0^1 \phi_i\,\phi_j'\,d\xi = \begin{cases} \frac{2ji}{j^2-i^2}[(-1)^{j+1}-1] & i \neq j,\\ 0 & i = j,\end{cases}\\
\alpha_{ijkl} &= \int_0^1 \phi_i\,\phi_j'' \int_0^1 \phi_k'\,\phi_l'\,d\xi\,d\xi,
\end{aligned} \tag{22}$$

4. Convergence analysis

Firstly, the number of modes (i.e., N) used in Galerkin technique should be determined to obtain convergent results. It should be mentioned that the required number to get convergent results is different for linear and nonlinear analyses. In the present study, $N = 4$ and $N = 8$ are chosen for linear and nonlinear analyses, respectively. The details for convergence analysis can be found in Appendix B.

Following the parameter values chosen in [Wang and Ni 2008] and [Li et al. 2015b], here we give $\varphi = 0.5$, $\beta = 0.2$, $\varepsilon = 50$, $\bar{c}_d = 0.002$, $c_f = 0.02$, $\overline{\gamma} = 0.002$, $\Gamma = 1$, $\dot{v} = 0$ for the present investigation. For the sake of simplicity, it should be noted that the parameter $\overline{\gamma}$ is given without over-bar in the following sections.

5. Linear dynamic analysis

In this section, numerical studies are performed to investigate the effects of moving speed, flow velocity and some parameters on stabilities and critical moving speed of the beam. Evolutions of the natural

frequency and damping of the beam system can be obtained through eigenvalue analysis and only the lowest three modes are presented here.

Before analyzing the results, three kinds of critical moving speed are defined:

v_{Bi}: the bifurcation critical moving speed at ith mode, at which the frequency of beam is decreased to zero.

v_{Di}: the divergence critical moving speed at ith mode, at which buckling behavior of the beam occurs.

v_{Fi}: the flutter critical moving speed at ith mode, at which flutter vibrations of the beam take place.

5.1. ***Effects of the flow velocity on stability of the beam system.*** Figure 3 shows the evolution of dimensionless damping (Im(ω)) and frequency (Re(ω)) varying with the moving speed of beam when the external flow velocity is $v_f = 5$. Inspecting Figure 3 (left), one can find that bifurcation and divergence (static buckling) behaviors of the beam in the first mode occur at $v_{B1} = 3.04$ and $v_{D1} = 3.05$, respectively. This indicates that the beam loses stability by buckling at the first mode when the moving speed is 3.05. Increasing the moving speed further, the beam loses stability by flutter at $v_{F1} = 5.96$ in the first mode and keeps this state of instability as v increases further. As to the second mode, the bifurcation behavior occurs at $v_{B2} = 8.71$ and the divergence occurs at $v_{D2} = 8.86$ where static buckling of the beam takes place. As the moving speed is increased to $v_{F2} = 11.73$, flutter of the beam occurs. In the third mode of the beam, it always maintains stability over the moving speed range. The corresponding frequency varying with the moving speed is displayed in Figure 3 (right), showing the bifurcation points at which the frequency is deceased to zero in the first and second mode of the beam.

In order to further understand variations of the critical moving speed of the beam with the external flow velocity (v_f), we plot in Figure 4 the variation for divergence and flutter critical moving speeds in the first and second modes. The flow velocity is in the range of $0 \le v_f \le 15$. Different kinds of critical moving speeds, namely, v_{D1}, v_{F1}, v_{D2} and v_{F2}, are shown. It is found that the critical moving speed (v_{D1} and v_{F1}) in the first mode is slightly increased first and then decreased, and finally it is slightly increased

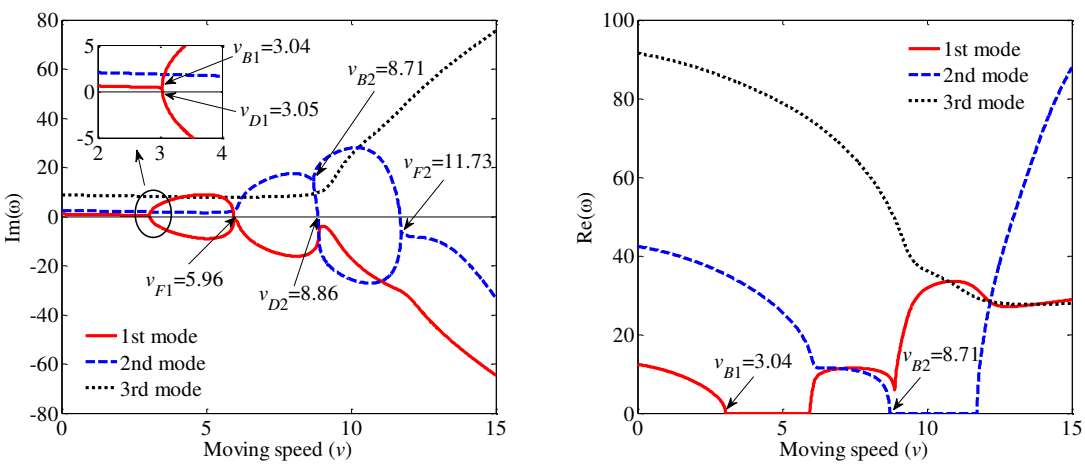

Figure 3. Evolutions of the damping (Im(ω)) and frequency (Re(ω)) of the beam with increasing the moving speed when $v_f = 5$.

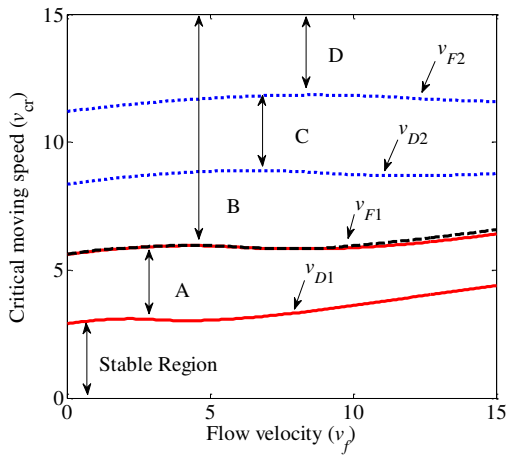

Figure 4. Stability diagram in the flow velocity-moving speed plane.

with the increase of flow velocity; while in the second mode, it changes a little with increasing the flow velocity. What is more, we offer the instability boundary varying with the flow velocity in Figure 4, which shows the instability characteristics of the beam.

In the considered flow velocity region from 0 to 15, when the moving speed is below the boundary of v_{D1}, the beam is stable. When the moving speed is beyond the boundary of v_{D1}, the beam displays several kinds of unstable modes. The instabilities involved can be divided into four regions which are described as follows:

Subregion A: in this region, between the two red lines, the beam loses stability by divergence, developing the static buckling in the first mode.

Subregion B: in this region, above the black dashed line, the beam loses stability by flutter in the first mode.

Subregion C: in this region, between the two blue dotted lines, the beam loses stability by divergence, developing static buckling in the second mode.

Subregion D: in this region, above the upper blue dotted line, the beam loses stability by flutter in the second mode.

5.2. ***Effects of other parameters on the first critical moving speed.*** In this subsection, the effects of parameters like the axial added mass coefficient β, slenderness ratio ε, mass ratio φ and pretension Γ on the critical moving speed are investigated. It should be pointed out that the instability of moving beam first occurs in the first mode via buckling, thus, v_{D1} is the critical moving speed v_{cr} when performing parametric analysis.

Four 3D plots are presented in Figure 5 to show the influences of β, ε, φ and Γ on the critical moving speed v_{cr}. Inspecting Figure 5 (top left), we can see that large flow velocity and small β gives a high critical moving speed of the beam. Specifically, the critical moving speed v_{cr} is reduced as β is increased, and the rate of reduction in the critical speed is faster as the flow velocity increased. By looking at Figure 5 (top right), one can find that the corner in the high values of ε and flow velocity region is high up, while the corner in the region of high flow velocity and low ε drops down. This indicates that

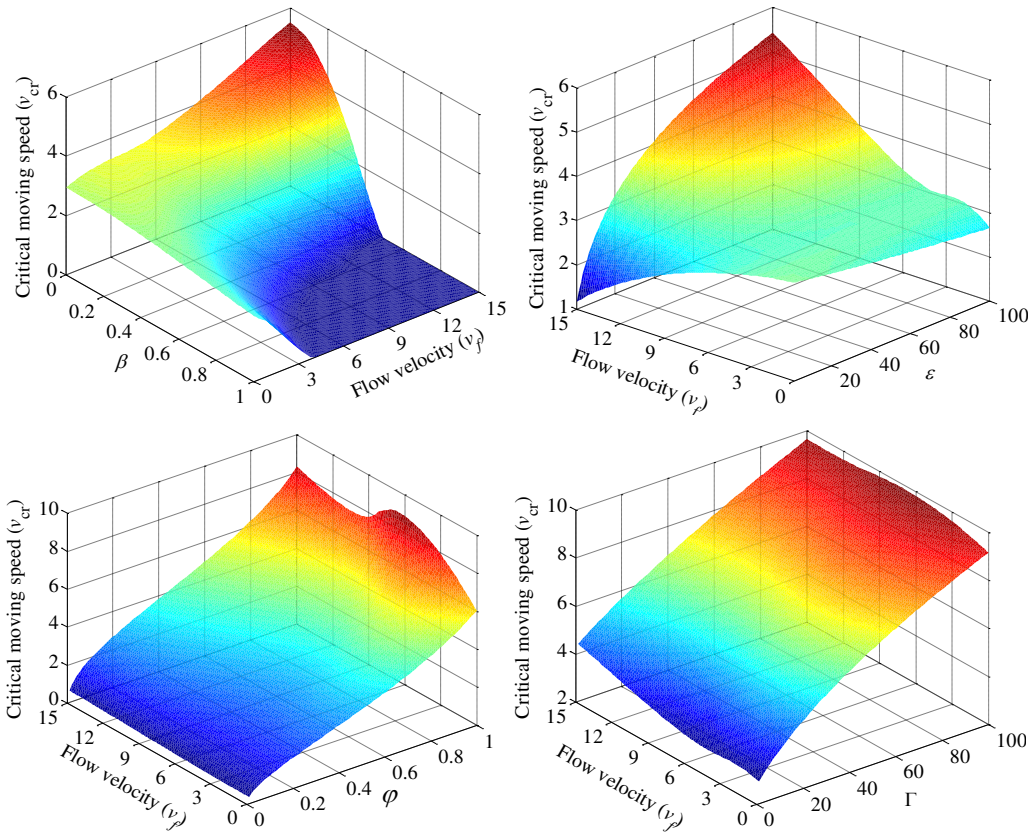

Figure 5. Critical moving speed v_{cr} as a function of the axial added mass coefficient β (top left); slenderness ratio ε (top right); mass ratio φ (bottom left); pretension Γ (bottom right) when varying the flow velocity (v_f) .

when the flow velocity (v_f) is high enough, a small slenderness ratio (ε) results in a low critical moving speed, while large slenderness ratio produces a high critical moving speed of the beam. The results in Figure 5 (bottom left and bottom right) respectively show that v_{cr} is increased for higher values of φ and Γ, while increasing the flow velocity gives a small increase in v_{cr}. In addition, the Kelvin–Voigt damping coefficient γ has no influence on the critical moving speed v_{cr}.

6. Nonlinear dynamic analysis

According to the linear analysis, it is noted that the beam can experience buckling and flutter with increasing moving speed. And parameters such as the axial added mass coefficient, slenderness ratio, mass ratio and pretension have a significant effect on the critical moving speed. However, linear analysis can only predict the dynamic behavior of the beam system, but cannot forecast its vibration response. So, nonlinear analysis is necessary to obtain the nonlinear vibration response of the beam.

6.1. ***General vibration response of the beam.*** Firstly, we focus on predicting vibration response of the beam with increasing moving speed for different values of the flow velocity. The Galerkin truncation

number is $N = 8$ to obtain convergent results (see Appendix B). The vibration response of the beam gained through nonlinear analysis is summarized via bifurcation diagrams where the vibration amplitude of the midpoint of the beam is recorded as a function of the moving speed v.

In the case of $v_f = 1$, the bifurcation diagram is shown in Figure 6 (top left). One can see that the beam system remains stable until $v = 3.0$ and the static buckling starts to occur at $v = 3.1$, as predicted by linear analysis. However, as the moving speed is increased to $v = 10.5$, the static buckling is transformed to flutter. At that time, the beam undergoes periodic or nonperiodic motions. Then the flutter instability ceases and the beam system is returned to static buckling at $v = 14.3$. The corresponding buckling and flutter responses can be found in the regions shown in the figure.

As the flow velocity is increased to $v_f = 2$, the bifurcation diagram is plotted in Figure 6 (top right). It is noted that the beam is stable for $v \leq 3.0$. However, with further increment of moving speed, static buckling instability occurs at $v = 3.1$, which is in conformity with linear theory. Then, the static buckling and flutter instability occur sequentially: static buckling instability for $3.1 \leq v \leq 10.6$ and flutter instability for $10.7 \leq v \leq 14.5$. When the flow velocity is equal to 3, we can find that buckling of the beam also occurs when the moving speed is between 3.1 and 10.6 and flutter occurs between 10.7 and 15.1. In summary, by inspecting Figure 6, we note that the buckling region of moving speed changes

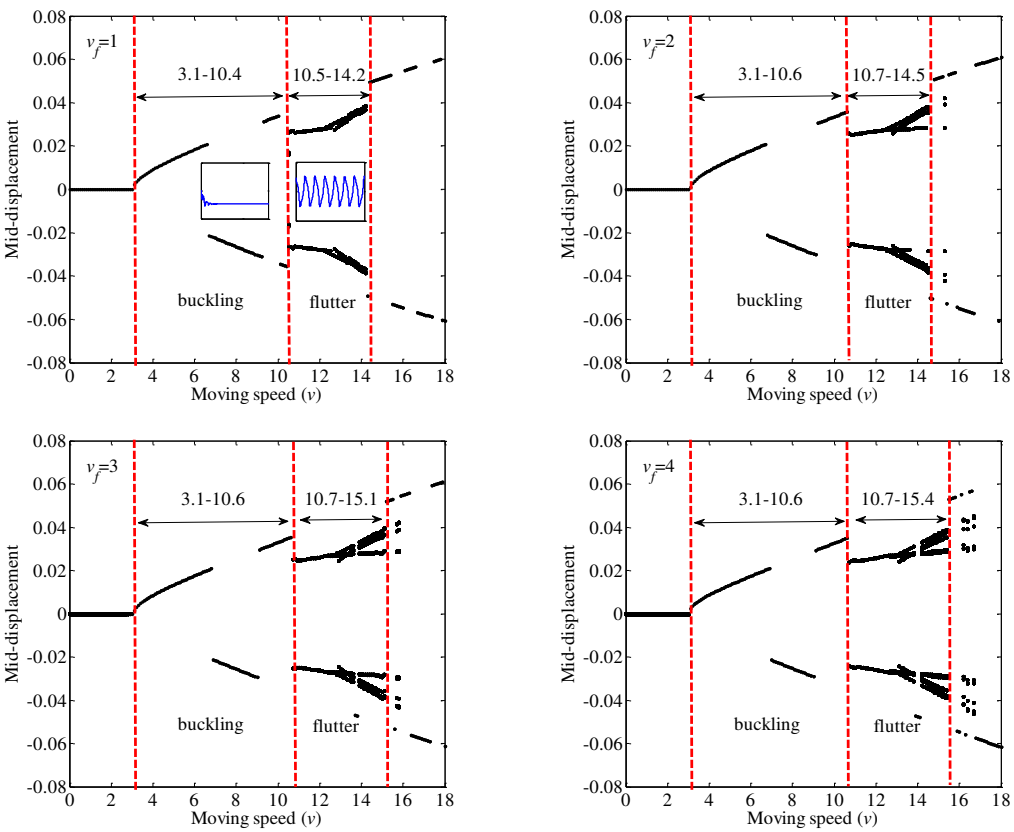

Figure 6. Bifurcation diagrams for the vibration amplitude of the beam when $v_f = 1$ (top left), $v_f = 2$ (top right), $v_f = 3$ (bottom left) and $v_f = 4$ (bottom right).

little while the flutter region of moving speed is a little increased when the flow velocity is increased from 1 to 4. In addition, for higher moving speeds, after the flutter region, it is noted that the responses are complex including flutter and buckling responses; also the flutter becomes clearer with the increase of flow velocity.

It is interesting to investigate how the dynamic responses of the beam vary with moving speed when the axial flow velocity is large enough (e.g., when v_f is beyond 7), as plotted in Figure 7. It is indicated that when flow velocity is increased to 7, the buckling moving speed is increased to 3.3, and the flutter responses occur at 11.7 till 14. Increasing the moving speed further, beyond 14, the beam then returns to buckling response. As the flow velocity is further increased to 8 and 9, we note that the critical moving speed is slightly increased to 3.4 and 3.5, and the buckling region is widened to 3.4–12.5 and 3.5–13.3, respectively. However, the flutter region is respectively decreased to 12.6–14.1 and 13.4–14.2. This indicates that increasing the flow velocity can eliminate the flutter response of the beam. Interestingly, as the flow velocity is increased to 11, the beam experiences totally a buckling response over the considered moving speed region.

It is concluded from figures 6 and 7 that the beam can undergo buckling and flutter motions with increasing moving speed v for different values of the axial flow velocity. However, when the flow

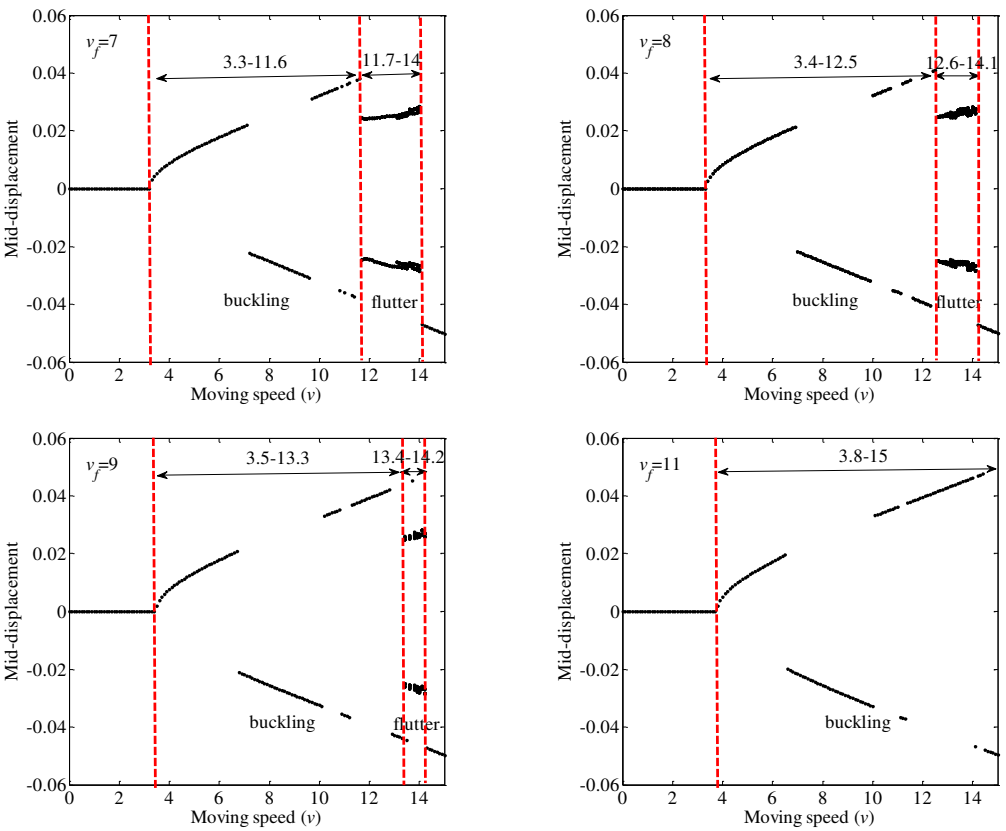

Figure 7. Bifurcation diagrams for the vibration amplitude of the beam when $v_f = 7$ (top left), $v_f = 8$ (top right), $v_f = 9$ (bottom left) and $v_f = 11$ (bottom right).

velocity is low (e.g., v_f is below 4), it has little effect on the buckling region but can increase the flutter region with the increase of flow velocity. In the case of large flow velocity (e.g., v_f beyond 7), the buckling region can be increased while the flutter region is decreased with increasing flow velocity.

6.2. ***Parametric analysis on buckling and flutter responses.*** In this subsection, the effects of several key parameters on the buckling and flutter responses of the beam system are examined and results are shown in figures 8–10. Figure 8 (top left) shows the bifurcation diagram of the beam for different values of the axial added mass coefficient β. It is seen that with increasing β the divergence point decreases, which agrees with the conclusion obtained by linear analysis. Also at a fixed moving speed, the amplitude of buckling is increased with larger values of axial added mass coefficient. Figure 8 (top right, bottom left and bottom right) show the bifurcation diagrams of the beam system for different values of the slenderness ratio ε , the mass ratio φ and the dimensionless pretension Γ, respectively. All these three figures show that, the larger the values of these three parameters are, the smaller the amplitudes of buckling become. As predicted by linear analysis, one can find that the critical moving speed at which divergence occurs increases with the increase of ε, φ, Γ, respectively.

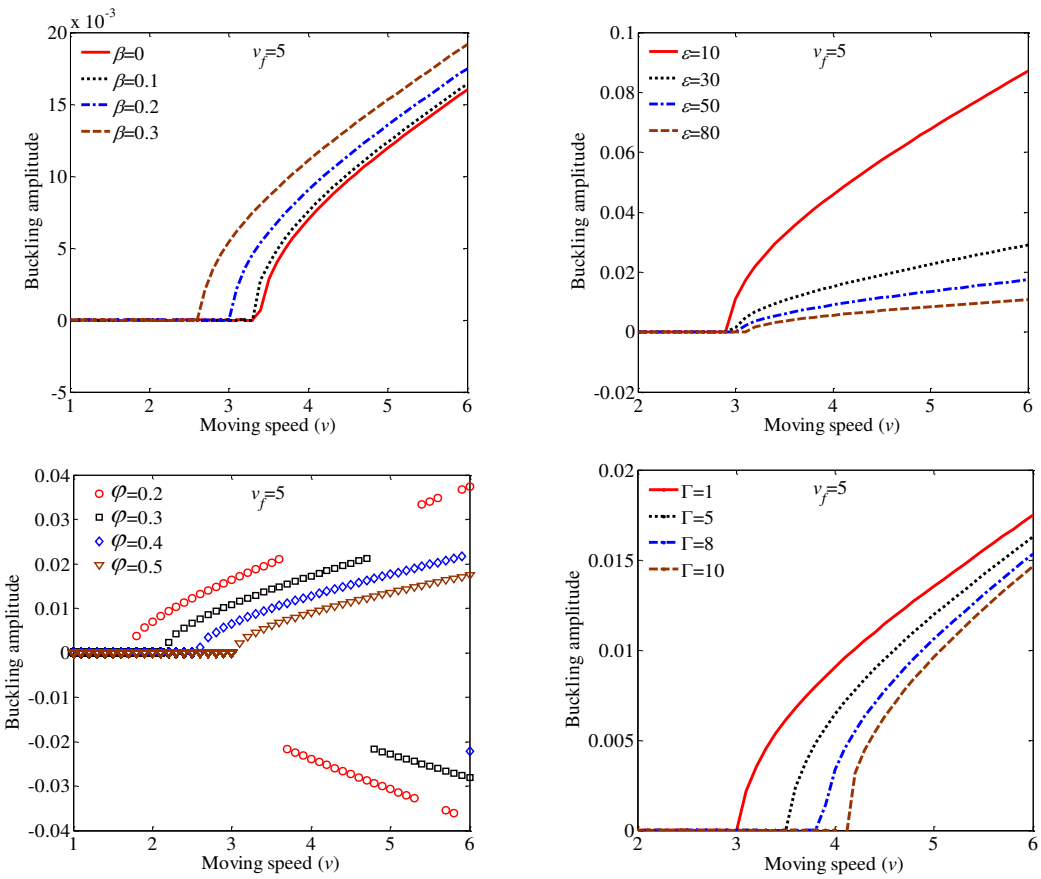

Figure 8. Bifurcation diagrams of the beam varying with β (top left); ε (top right); φ (bottom left); Γ (bottom right).

For fixed values of axial flow velocity and moving speed, Figure 9 shows the bifurcation diagrams of the beam as these key parameters are varied, for $v_f = 5$ and $v = 11$. We note the beam can experience buckling and flutter responses with increasing the axial added mass coefficient β and the slenderness ratio ε, as indicated in Figure 9 (top row). For example, when β is below 0.18, the beam is subjected to buckling. For β beyond 0.18, flutter responses of the beam occurs, but the vibration amplitude changes little. The instability type is transferred from buckling to flutter at $\varepsilon = 45$. The corresponding amplitudes are decreased with the increase of ε. It is noted from Figure 9 (bottom left) that the mass ratio φ has a great impact on the vibration amplitude of the moving beam, resulting in a clear reduction of amplitude with increasing the mass ratio. As to the effect of the pretension Γ, we note that the beam undergoes flutter over the considered region and the vibration amplitude is a little decreased with the increase of Γ.

The Kelvin–Voigt damping γ has no influence on the critical moving speed, as mentioned in the previous section. Here we study whether it has an effect on the vibration amplitude of the beam, as plotted in Figure 10. Indeed, γ has no effect on the buckling amplitude, as seen in Figure 10 (left). This can be expected from the equation of motion, showing that γ is always associated with time-dependent terms. By looking at Figure 10 (right), one can find that the beam system jumps from periodic responses

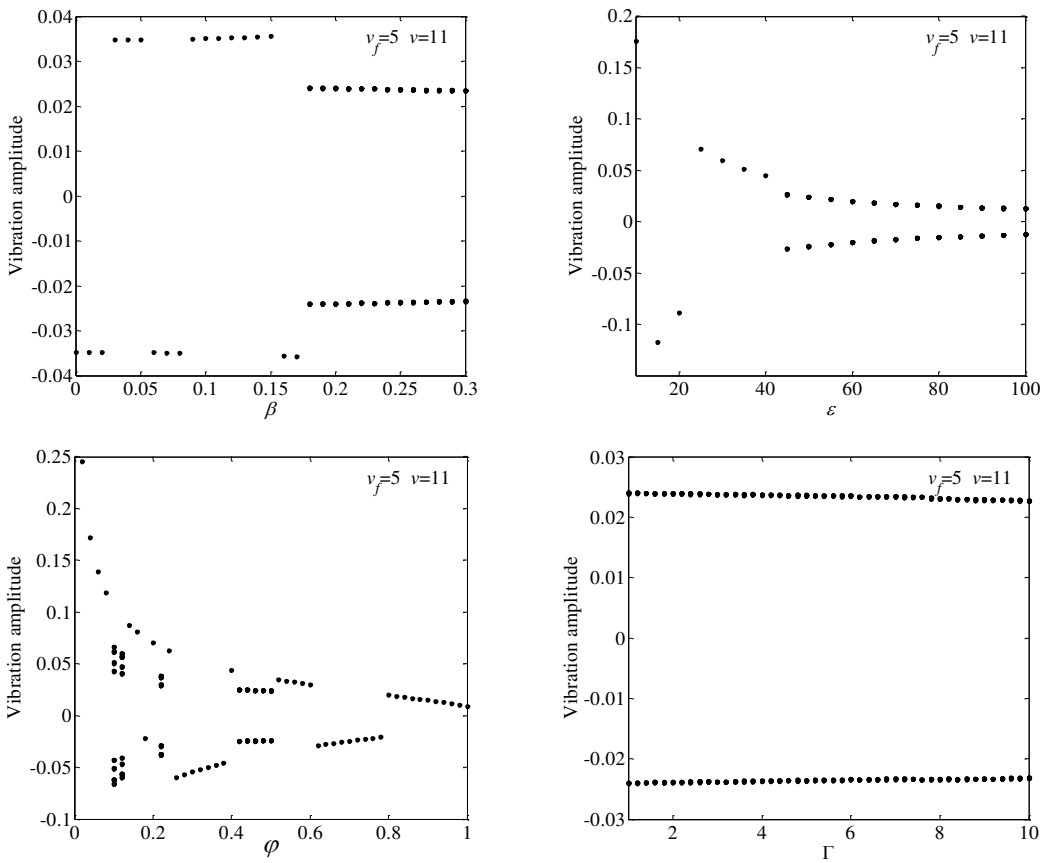

Figure 9. Bifurcation diagrams of the beam varying with β (top left); ε (top right); φ (bottom left); Γ (bottom right) when $v_f = 5$ and $v = 11$ throughout.

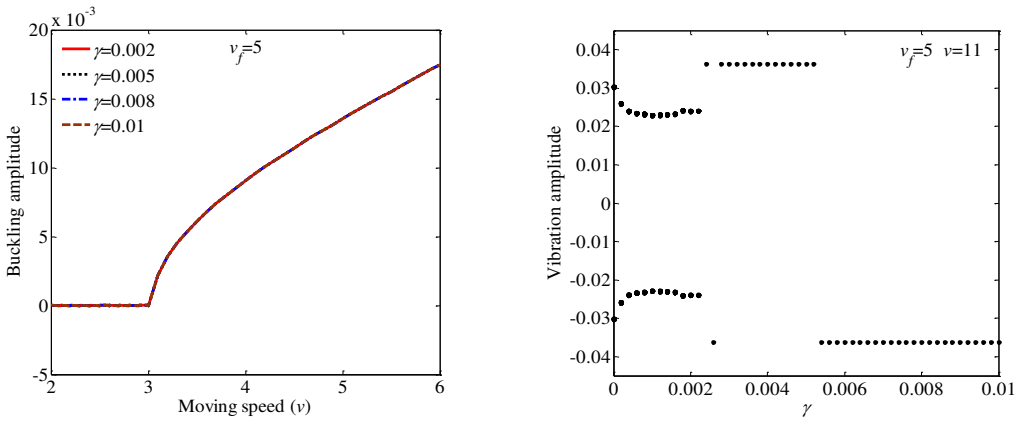

Figure 10. Bifurcation diagrams of the beam for different values of γ when $v_f = 5$ (left) and with increasing γ when $v_f = 5$ and $v = 11$ throughout (right).

to buckling when γ is increased to 0.0022. Moreover, the flutter amplitude is decreased as γ increases, while the buckling amplitude remains unchanged with increasing γ. The performed parametric analysis offers a significant insight into the sensitivity of the dynamic responses of the axially moving beam system on the parameters considered.

7. Conclusions

In this work, a nonlinear dynamic model for an axially moving beam subjected to external axial flow was established. The nonlinear vibrations and stability analysis of the moving beam were investigated in detail, considering the effects of system parameters such as the flow velocity, axial added mass coefficient, mass ratio, slenderness ratio, pretension and the Kelvin–Voigt damping. Results show that the critical moving speed where the instability of beam occurs is obviously affected by the system parameters for different values of flow velocity. The vibration characteristics of the moving beam can also be significantly affected by variation of the system parameters, showing a transition behavior between buckling and flutter responses. Some important conclusions can be drawn out as follows:

(1) It is noted that parameters such as axial added mass coefficient and slenderness ratio have great effects on the critical moving speed of beam, and their influences vary with flow velocity. However, increasing the mass ratio and pretension leads to an increase of the critical moving speed, which can be slightly affected by the flow velocity.

(2) When the flow velocity is low, it has little impact on the buckling region of moving speed, while the flutter region can be widened for increasing flow velocity. When the flow velocity is large enough, the flutter region of moving speed is gradually decreased and the beam may only undergo buckling over the moving speed with increasing flow velocity.

(3) The vibration responses of the beam are sensitive to the axial added mass coefficient, slenderness ratio, mass ratio and pretension. However, Kelvin–Voigt damping has no influence on the buckling response of the beam.

Appendix A. The derivation of the general expressions for the viscous forces

In this section, the general expressions for the F_N and F_L are derived in detail. Owing to the axial external flow is in x-direction, the free-stream velocity and the beam velocity can be expressed as [Kheiri et al. 2013a]

$$\vec{V}_{f,\infty} = V_f \boldsymbol{i}, \tag{A.1}$$

$$\vec{V}_b = V_{bx}\,\boldsymbol{i} + V_{by}\,\boldsymbol{j} = (\dot{v} + V + Vu')\boldsymbol{i} + (\dot{w} + Vw')\,\boldsymbol{j}, \tag{A.2}$$

where V_{bx} and V_{by} are components of $\vec{V}_b$ along the x- and y-directions, and the over-dot and the prime denote the derivative with respect to time and x. And w, $\dot{w}$, $w' \sim O(\varepsilon)$ and u, $\dot{u}$, $u' \sim O(\varepsilon^2)$.

The relative velocity between the free-stream and the beam can be easily obtained as

$$\vec{V}_{f/b} = (V_f - V_{bx})\boldsymbol{i} - V_{by}\,\boldsymbol{i}. \tag{A.3}$$

Therefore, the magnitude of the relative fluid-beam velocity can be written as

$$|\vec{V}_{f/b}| = V_f\left[\left(1 - \frac{V_{bx}}{V_f}\right)^2 + \left(\frac{V_{by}}{V_f}\right)^2\right]^{1/2}. \tag{A.4}$$

From Figure 11, the relative fluid-beam velocity $\vec{V}_{f/b}$ can be decomposed into an axial component $\vec{V}_a$ and a normal component $\vec{V}_c$; i is the angle of incidence angle; θ is the angle between the longitudinal axis of the beam with the x-axis. The axial and normal components of $\vec{V}_{f/b}$ may be expressed as

$$\vec{V}_a = |\vec{V}_a|\big((1+u')\boldsymbol{i} + w'\boldsymbol{j}\big), \tag{A.5}$$

$$\vec{V}_c = |\vec{V}_c|(a\boldsymbol{i} + b\boldsymbol{j}), \tag{A.6}$$

where the vectors given in bars are unit tangential vectors, hence $(1+u')^2 + w'^2 = 1$ and $a^2 + b^2 = 1$.

By using (A.3), (A.5) and (A.6), one obtains

$$|\vec{V}_a|(1+u') + |\vec{V}_c|a = V_f - V_{bx}, \quad |\vec{V}_a|w' + |\vec{V}_c|b = -V_{by}. \tag{A.7}$$

Adding the squares of the equations in (A.7) and using the relationship $|\vec{V}_{f/b}|^2 = |\vec{V}_a|^2 + |\vec{V}_c|^2$, the magnitude of axial flow velocity can be obtained as

$$|\vec{V}_a| = (1+u')(V_f - V_{bx}) - w'V_{by}. \tag{A.8}$$

According to Figure 11, one can write

$$|\cos i| = \frac{|\vec{V}_a|}{|\vec{V}_{f/b}|}, \quad |\sin i| = \frac{|\vec{V}_c|}{|\vec{V}_{f/b}|}. \tag{A.9}$$

From (A.4), (A.8) and $(A.9)_1$, using $(1+u') = 1 - \frac{1}{2}w'^2 + O(\varepsilon^4)$ and after neglecting the high-order terms, one can get

$$|\cos i| = 1 - \frac{1}{2}\left(w' + \frac{\dot{w} + Vw'}{V_f - V_{bx}}\right)^2 + O(\varepsilon^4). \tag{A.10}$$

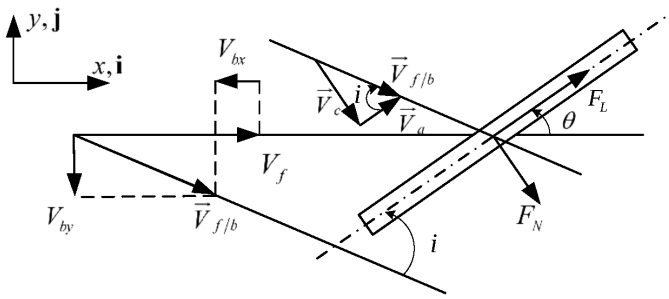

Figure 11. The beam element subjected to viscous forces.

According to Taylor's work, F_N and F_L can be expressed by (5) and (6). It is worth to point that the U in (5) and (6) is the axial external flow velocity in the stationary beam case. For this particular case (i.e., with the beam axially moving in axial external flow), one should consider the effect both of the axial external flow and the axial moving speed of the beam itself, hence U can be considered as the relative velocity between fluid and beam, i.e., $\vec{V}_{f/b}$. Then the viscous forces can be rewritten as

$$F_L = \frac{1}{2}\rho D(\vec{V}_{f/b})^2 C_f \cos i, \quad F_N = \frac{1}{2}\rho D(\vec{V}_{f/b})^2 (C_f \sin i + C_{D_p} \sin^2 i). \tag{A.11}$$

Substituting (A.10) into $(A.11)_1$, one can obtain

$$F_L = \frac{1}{2}\rho D(\vec{V}_{f/b})^2 C_f \left[1 - \frac{1}{2}\left(w' + \frac{\dot{w} + V w'}{V_f - V_{bx}}\right)^2\right]. \tag{A.12}$$

In order to derive the expression for normal viscous force conveniently, F_N is decomposed into two parts: the friction drag term $F_{N,f}$ and the form drag term $F_{N,fd}$ which can be expressed as

$$F_{N,f} = \frac{1}{2}\rho D(\vec{V}_{f/b})^2 C_f |\sin i|, \quad F_{N,fd} = \frac{1}{2}\rho D(\vec{V}_{f/b})^2 C_{D_p} \sin^2 i. \tag{A.13}$$

The y-component and x-component of $F_{N,f}$ become

$$(F_{N,f})_y = F_{N,f}\left(\frac{\vec{V}_c}{|\vec{V}_c|} \cdot \boldsymbol{j}\right), \quad (F_{N,f})_x = F_{N,f}\left(\frac{\vec{V}_c}{|\vec{V}_c|} \cdot \boldsymbol{i}\right). \tag{A.14}$$

From (A.4), $(A.7)_2$, (A.8), $(A.9)_2$, $(A.13)_1$, $(A.14)_1$ and after many tedious manipulations, we can obtain

$$(F_{N,f}) = -\frac{1}{2}\rho D(\vec{V}_{f/b})^2 C_f \left[w' + \frac{\dot{w} + V w'}{V_f - V_{bx}} - w'^2\left(\frac{\dot{w} + V w'}{V_f - V_{bx}}\right) - \frac{1}{2}w'\left(\frac{\dot{w} + V w'}{V_f - V_{bx}}\right)^2 - \frac{1}{2}w'^3 - \frac{1}{2}\left(\frac{\dot{w} + V w'}{V_f - V_{bx}}\right)^3\right]. \tag{A.15}$$

The minus sign in (A.15) arises because the force was considered to be generally in the positive direction. The minus sign can be removed if F_N is considered with the sign convention shown in Figure 11.

In the same spirit as (A.15) for $(F_{N,f})_y$, from (A.4), (A.7)$_1$, (A.8), (A.9)$_2$, (A.13)$_1$, (A.14)$_2$, $(F_{N,f})_x$ can be expressed as

$$(F_{N,f})_x = \frac{1}{2}\rho D(\vec{V}_{f/b})^2 C_f\left[w'^2 + \frac{w'(\dot{w}+Vw')}{V_f - V_{bx}}\right]. \tag{A.16}$$

From (A.10), one can obtain

$$\sin^2 i = 1 - \cos^2 i \approx \left(w' + \frac{\dot{w}+Vw'}{V_f - V_{bx}}\right)^2. \tag{A.17}$$

Substituting (A.17) into (A.13)$_2$, $F_{N,fd}$ can be expressed as

$$F_{N,fd} = \frac{1}{2}\rho D(\vec{V}_{f/b})^2 C_{D_p}\left(w' + \frac{\dot{w}+Vw'}{V_f - V_{bx}}\right)^2. \tag{A.18}$$

The y-component and x-component of $F_{N,fd}$ can be easily obtained:

$$(F_{N,fd})_y = F_{N,fd}\cos\theta \approx \frac{1}{2}\rho D(\vec{V}_{f/b})^2 C_{D_p}\left(w' + \frac{\dot{w}+Vw'}{V_f - V_{bx}}\right)^2, \tag{A.19}$$

$$(F_{N,fd})_x = F_{N,fd}\sin\theta \approx \frac{1}{2}\rho D(\vec{V}_{f/b})^2 C_{D_p} w'\left(w' + \frac{\dot{w}+Vw'}{V_f - V_{bx}}\right)^2. \tag{A.20}$$

Then, the expressions for the y-component and x-component of F_N, denoted by F_{Ny} and F_{Nx}, respectively, can be expressed as

$$\begin{aligned} F_{Ny} = {} & \frac{1}{2}\rho D(\vec{V}_{f/b})^2 \\ & \times \left\{ C_f\left[w' + \frac{\dot{w}+Vw'}{V_f - V_{bx}} - w'^2\left(\frac{\dot{w}+Vw'}{V_f - V_{bx}}\right) - \frac{1}{2}w'\left(\frac{\dot{w}+Vw'}{V_f - V_{bx}}\right)^2 - \frac{1}{2}w'^3 - \frac{1}{2}\left(\frac{\dot{w}+Vw'}{V_f - V_{bx}}\right)^3\right] \right. \\ & \left. + C_{D_p}\left(w' + \frac{\dot{w}+Vw'}{V_f - V_{bx}}\right)\right\}, \end{aligned} \tag{A.21}$$

$$F_{Nx} = \frac{1}{2}\rho D(\vec{V}_{f/b})^2\left[C_f\left(w'^2 + \frac{w'(\dot{w}+Vw')}{V_f - V_{bx}}\right) + C_{D_p} w'\left(w' + \frac{\dot{w}+Vw'}{V_f - V_{bx}}\right)^2\right]. \tag{A.22}$$

The component of $\vec{V}_{f/b}$ along y-axis is small compared with the component along x-axis and the axial displacement of beam $u(x,t)$ is of order $O(\varepsilon^2)$, hence we can write $\vec{V}_{f/b}^2 = (V_f - V_{bx})^2 + V_{by}^2 \approx (V_f - V_{bx})^2$ and $V_{bx} \approx V$. Recalling $V_{by} = \dot{w} + Vw'$ and according to Gosselin et al. [2007], the $V_{by\max}$ is given by the relationship $V_{by}^3 \cong V_{by}^2 V_{by\max}(8/3\pi)$. Substituting these relationships into (A.12), (A.21) and (A.22), and after some linearization procedures, one obtains

$$F_L = \frac{1}{2}\frac{m_v}{D}(V_f - V)^2 c_f, \quad F_{Ny} = \frac{1}{2}\frac{m_v}{D}c_f(V_f - V)(\dot{w} + V_f w') + \frac{1}{2}\frac{m_v}{D}c_d(\dot{w} + Vw'), \tag{A.23}$$

where $c_f = (4/\pi)C_f$, $c_d = (4/\pi)(8V_{by\max}/3\pi)C_{D_p}$ and $m_v = \frac{1}{2}\rho D^2\pi$. Furthermore, $F_{Nx} \sim O(\varepsilon^2)$ can be neglected.

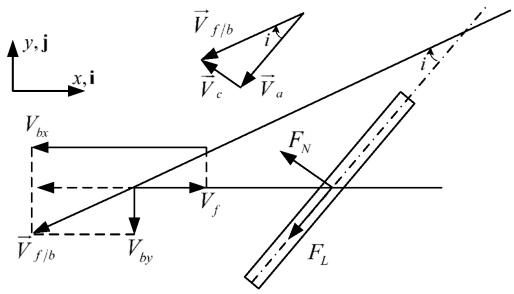

Figure 12. The beam element subjected to viscous forces when $V_f < V_{bx}$.

Considering the condition of $V_f < V_{bx}$, which is shown in Figure 12, the directions of F_L and F_N turn opposite. Recalling (A.15), the minus sign can be kept under this situation. Hence, the general linearized expressions for the viscous forces can be obtained:

$$F_L = \frac{1}{2}\frac{m_v}{D}(V_f - V)^2 c_f \,\mathrm{sgn}(V_f - V), \quad F_{Ny} = \frac{1}{2}\frac{m_v}{D}\big(c_f|V_f - V|(\dot{w} + V_f w') + c_d(\dot{w} + V w')\big), \tag{A.24}$$

where $\mathrm{sgn}(V_f - V)$ is a sgn function, i.e., $\mathrm{sgn}(V_f - V) = 1$ if $V_f > V$; $\mathrm{sgn}(V_f - V) = -1$ if $V_f < V$; $\mathrm{sgn}(V_f - V) = 0$ if $V_f = V$.

Appendix B. The determination of Galerkin truncation number N

In linear analysis, the critical speeds v_{cr} for different flow velocities are checked in the convergence tests to be discussed. Figure 13 shows the critical values of the moving speed v_{cr} as a function of the axial flow velocity, and the four curves represent results which are obtained with $N = 3, 4, 5$ and 6, respectively. One can find that these four curves are highly coincident with each other. Thus, $N = 4$ is an optimal choice from the point of a view of reliability and computational efficiency.

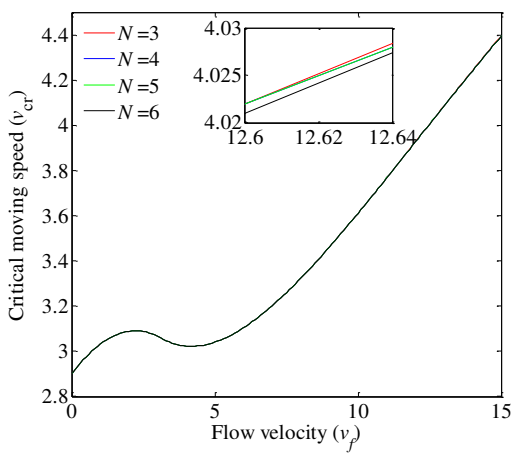

Figure 13. Critical speed v_{cr} as function of the flow velocity for different Galerkin truncation numbers N.

Furthermore, the Galerkin truncation number N for obtaining reliable nonlinear dynamic responses can be determined by inspecting Figure 14. In the case of $v_f = 0$, we choose $N = 4, 6$ and 8 in the numerical calculations (see Figure 14, left column). In the case of $v_f = 5$, we choose $N = 6, 8$ and 10 (see Figure 14, right column). As can be observed, $N = 8$ can be chosen to ensure the reliability of results in the nonlinear analysis.

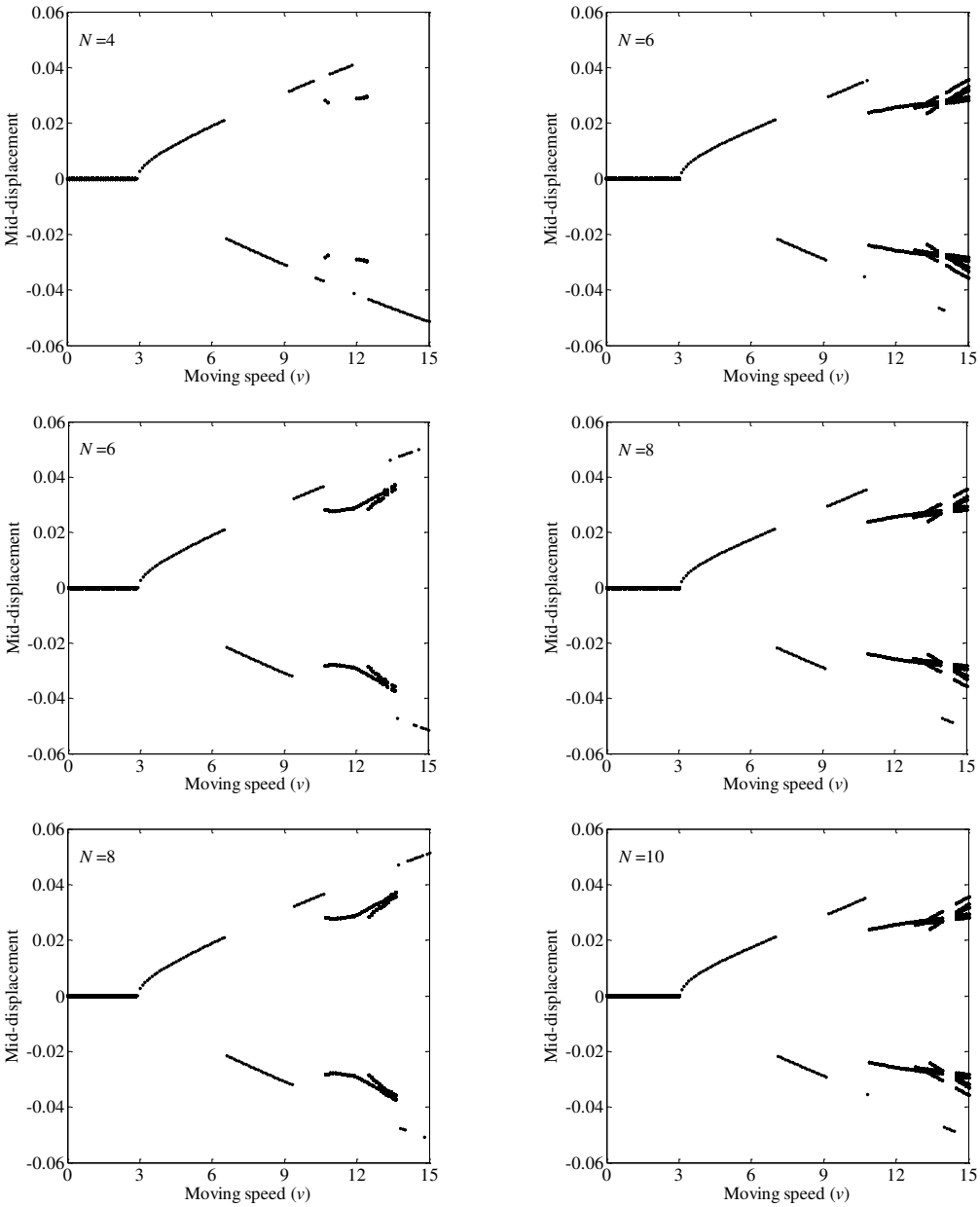

Figure 14. Bifurcation diagrams for the cases $v_f = 0$ (left column) and $v_f = 5$ (right column) by using different Galerkin truncation numbers N.

Acknowledgment

The financial support of the National Natural Science Foundation of China (No. 11672115, No. 11622216, No. 11602090 and No. 11902229) to this work is gratefully acknowledged.

References

[Banichuk et al. 2010] N. Banichuk, J. Jeronen, P. Neittaanmäki, and T. Tuovinen, "Static instability analysis for travelling membranes and plates interacting with axially moving ideal fluid", *J. Fluid. Struct.* **26**:2 (2010), 274–291.

[Banichuk et al. 2011] N. Banichuk, J. Jeronen, P. Neittaanmäki, and T. Tuovinen, "Dynamic behaviour of an axially moving plate undergoing small cylindrical deformation submerged in axially flowing ideal fluid", *J. Fluid. Struct.* **27**:7 (2011), 986–1005.

[Brown 2006] R. J. Brown, "Past, present, and future towing of pipelines and risers", pp. document id. OTC–18047–MS in *Offshore Technology Conference* (Texas), 2006.

[Chen 2005] L.-Q. Chen, "Analysis and control of transverse vibrations of axially moving strings", *Appl. Mech. Rev.* (*ASME*) **58**:2 (2005), 91–116.

[Chen et al. 2009] L.-Q. Chen, W. Zhang, and J. W. Zu, "Nonlinear dynamics for transverse motion of axially moving strings", *Chaos Solitons Fractals* **40**:1 (2009), 78–90.

[De Langre et al. 2007] E. De Langre, M. P. Païdoussis, O. Doaré, and Y. Modarres-Sadeghi, "Flutter of long flexible cylinders in axial flow", *J. Fluid Mech.* **571** (2007), 371–389.

[Dowling 1988] A. P. Dowling, "The dynamics of towed flexible cylinders, Part 1: neutrally buoyant elements", *J. Fluid Mech.* **187** (1988), 507–532.

[Frondelius et al. 2006] T. Frondelius, H. Koivurova, and A. Pramila, "Interaction of an axially moving band and surrounding fluid by boundary layer theory", *J. Fluid. Struct.* **22**:8 (2006), 1047–1056.

[Ghayesh 2012] M. H. Ghayesh, "Stability and bifurcations of an axially moving beam with an intermediate spring support", *Nonlinear Dyn.* **69** (2012), 193–210.

[Ghayesh et al. 2013a] M. H. Ghayesh, M. Amabili, and H. Farokhi, "Coupled global dynamics of an axially moving viscoelastic beam", *Int. J. Non-Linear Mech.* **51** (2013), 54–74.

[Ghayesh et al. 2013b] M. H. Ghayesh, M. Amabili, and M. P. Païdoussis, "Nonlinear dynamics of axially moving plates", *J. Sound Vib.* **332**:2 (2013), 391–406.

[Gosselin et al. 2007] F. Gosselin, M. P. Païdoussis, and A. K. Misra, "Stability of a deploying/extruding beam in dense fluid", *J. Sound Vib.* **299**:1-2 (2007), 123–142.

[Hedrih 2007] K. S. Hedrih, "Transversal vibrations of the axially moving sandwich belts", *Arch. Appl. Mech.* **77** (2007), 523–539.

[Huo and Wang 2016] Y. Huo and Z. Wang, "Dynamic analysis of a vertically deploying/retracting cantilevered pipe conveying fluid", *J. Sound Vib.* **360** (2016), 224–238.

[Kheiri et al. 2013a] M. Kheiri, M. P. Païdoussis, M. Amabili, and B. I. Epureanu, "Three-dimensional dynamics of long pipes towed underwater, Part 1: the equations of motion", *Ocean Eng.* **64** (2013), 153–160.

[Kheiri et al. 2013b] M. Kheiri, M. P. Païdoussis, M. Amabili, and B. I. Epureanu, "Three-dimensional dynamics of long pipes towed underwater, Part 2: linear dynamics", *Ocean Eng.* **64** (2013), 161–173.

[Kheiri et al. 2013c] M. Kheiri, M. P. Païdoussis, and A. M., "A nonlinear model for a towed flexible cylinder", *J. Sound Vib.* **332**:2 (2013), 1789–1806.

[Kheiri et al. 2015] M. Kheiri, M. P. Païdoussis, and M. Amabili, "An experimental study of dynamics of towed flexible cylinders", *J. Sound Vib.* **348** (2015), 149–166.

[Kim and Perkins 2002] W.-J. Kim and N. C. Perkins, "Two-dimensional vortex-induced vibration of cable suspensions", *J. Fluid. Struct.* **16**:2 (2002), 229–245.

[Kyriakides and Corona 2007] S. Kyriakides and E. Corona, *Mechanics of offshore pipelines: buckling and collapse*, vol. 1, Elsevier Science, 2007.

[Li et al. 2013] J. Li, X. H. Guo, J. Luo, and Y. Q. Li, H. Y. Wang, "Analytical study on inherent properties of a unidirectional vibrating steel strip partially immersed in fluid", *Shock Vib.* **20** (2013), 793–807.

[Li et al. 2015a] H. Y. Li, J. Li, and Y. J. Liu, "Internal resonance of an axially moving unidirectional plate partially immersed in fluid under foundation displacement excitation", *J. Sound Vib.* **358** (2015), 124–141.

[Li et al. 2015b] M. Li, Q. Ni, and L. Wang, "Nonlinear dynamics of an underwater slender beam with two axially moving supports", *Ocean Eng.* **108** (2015), 402–415.

[Li et al. 2018] H. Y. Li, J. Li, T. Y. Lang, and X. Zhu, "Dynamics of an axially moving unidirectional plate partially immersed in fluid under two frequency parametric excitation", *Int. J. Non-Linear Mech.* **99** (2018), 31–39.

[Lighthill 1960] M. J. Lighthill, "Note on the swimming of slender fish", *J. Fluid Mech.* **9**:2 (1960), 305–317.

[Lopes et al. 2002] J. L. Lopes, M. P. Païdoussis, and C. Semler, "Linear and nonlinear dynamics of cantilevered cylinders in axial flow, Part 2: the equations of motion", *J. Fluid. Struct.* **16**:6 (2002), 715–737.

[Marynowski and Kapitaniak 2014] K. Marynowski and T. Kapitaniak, "Dynamics of axially moving continua", *Int. J. Mech. Sci.* **81** (2014), 26–41.

[Mote Jr. 1968] C. D. Mote Jr., "Dynamic stability of an axially moving band", *J. Franklin Inst.* **285**:5 (1968), 329–346.

[Ni et al. 2014] Q. Ni, M. Li, M. Tang, and L. Wang, "Free vibration and stability of a cantilever beam attached to an axially moving base immersed in fluid", *J. Sound Vib.* **333**:9 (2014), 2543–2555.

[Païdoussis 1968] M. P. Païdoussis, "Stability of towed, totally submerged flexible cylinders", *J. Fluid Mech.* **34**:2 (1968), 273–297.

[Païdoussis 1970] M. P. Païdoussis, "Dynamics of submerged towed cylinders", pp. 981–1016 in *Eighth symposium on naval hydrodynamics: hydrodynamics in the ocean environment*, 1970.

[Païdoussis 1998] M. P. Païdoussis, *Fluid-structure interactions: slender structures and axial flow*, vol. 1, Academic Press, 1998.

[Païdoussis 2016] M. P. Païdoussis, *Fluid-structure interactions: slender structures and axial flow*, vol. 2, 2nd ed., Academic Press, 2016.

[Païdoussis and Li 1993] M. P. Païdoussis and G. X. Li, "Pipes conveying fluid: a model dynamical problem", *J. Fluid. Struct.* **7**:2 (1993), 137–204.

[Païdoussis et al. 2002] M. P. Païdoussis, E. Grinevich, D. Adamovic, and C. Semler, "Linear and nonlinear dynamics of cantilevered cylinders in axial flow, Part 1: physical dynamics", *J. Fluid. Struct.* **16**:6 (2002), 691–713.

[Semler et al. 2002] C. Semler, J. L. Lopes, N. Augu, and M. P. Païdoussis, "Linear and nonlinear dynamics of cantilevered cylinders in axial flow, Part 3: nonlinear dynamics", *J. Fluid. Struct.* **16**:6 (2002), 739–759.

[Taleb and Misra 1981] I. A. Taleb and A. K. Misra, "Dynamics of an axially moving beam submerged in a fluid", *J. Hydronautics* **15**:1 (1981), 62–66.

[Taylor 1952] G. I. Taylor, "Analysis of the swimming of long and narrow animals", *Proc. R. Soc. Lond. A* **214**:1117 (1952), 158–183.

[Telford et al. 1976] W. M. Telford, L. P. Geldart, R. E. Sheriff, and D. A. Key, *Applied geophysics*, Cambridge University Press, 1976.

[Wang 2018] Y. Q. Wang, "Electro-mechanical vibration analysis of functionally graded piezoelectric porous plates in the translation state", *Acta Astronaut.* **143** (2018), 263–271.

[Wang and Ni 2008] L. Wang and Q. Ni, "Vibration and stability of an axially moving beam immersed in fluid", *Int. J. Solids Struct.* **45**:5 (2008), 1445–1457.

[Wang and Zu 2017a] Y. Q. Wang and J. W. Zu, "Instability of viscoelastic plates with longitudinally variable speed and immersed in ideal liquid", *Int. J. Appl. Mech.* **9**:1 (2017), 1750005.

[Wang and Zu 2017b] Y. Q. Wang and J. W. Zu, "Vibration behaviors of functionally graded rectangular plates with porosities and moving in thermal environment", *Aerosp. Sci. Technol.* **69** (2017), 550–562.

[Wang et al. 2016] Y. Q. Wang, X. B. Huang, and J. Li, "Hydroelastic dynamic analysis of axially moving plates in continuous hot-dip galvanizing process", *Int. J. Mech. Sci.* **110** (2016), 201–216.

[Wickert and Mote 1988] J. A. Wickert and C. D. Mote, "Current research on the vibration and stability of axially-moving materials", *Shock Vib. Digest* **20**:5 (1988), 3–13.

[Yan et al. 2016] H. Yan, Q. Ni, H. L. Dai, L. Wang, M. Li, Y. Wang, and Y. Luo, "Dynamics and stability of an extending beam attached to an axially moving base immersed in dense fluid", *J. Sound Vib.* **383** (2016), 364–383.

[Yan et al. 2018] H. Yan, H. Dai, Q. Ni, L. Wang, and Y. Wang, "Nonlinear dynamics of a sliding pipe conveying fluid", *J. Fluid. Struct.* **81** (2018), 36–57.

Received 15 Apr 2019. Revised 25 Dec 2019. Accepted 29 Dec 2019.

YAN HAO: 824174017@qq.com
Wuhan Second Ship Design and Research Institute, Wuhan, 430205, China

HULIANG DAI: daihulianglx@hust.edu.cn
Department of Mechanics, Huazhong University of Science and Technology, Wuhan, 430074, China

NI QIAO: niqiao@hust.edu.cn
Department of Mechanics, Huazhong University of Science and Technology, Wuhan, 430074, China

KUN ZHOU: 2524642385@qq.com
Department of Mechanics, Huazhong University of Science and Technology, Wuhan, 430074, China

LIN WANG: wanglindds@hust.edu.cn
Department of Mechanics, Huazhong University of Science and Technology, Wuhan, 430074, China

JOURNAL OF MECHANICS OF MATERIALS AND STRUCTURES

msp.org/jomms

Founded by Charles R. Steele and Marie-Louise Steele

Cover photo: Ev Shafrir

See msp.org/jomms for submission guidelines.

JoMMS (ISSN 1559-3959) at Mathematical Sciences Publishers, 798 Evans Hall #6840, c/o University of California, Berkeley, CA 94720-3840, is published in 10 issues a year. The subscription price for 2020 is US $660/year for the electronic version, and $830/year (+$60, if shipping outside the US) for print and electronic. Subscriptions, requests for back issues, and changes of address should be sent to MSP.

JoMMS peer-review and production is managed by EditFLOW® from Mathematical Sciences Publishers.

PUBLISHED BY

mathematical sciences publishers

nonprofit scientific publishing

http://msp.org/

Journal of Mechanics of Materials and Structures

Volume 15, No. 1 January 2020